2023 IEEE/RSJ International Conference on Intelligent Robots and Systems (IROS)
October 1-5, 2023. Detroit, USA

Dynamic Multi-Target Tracking Using Heterogeneous Coverage Control

Ruoyu Lin† and Magnus Egerstedt†

***Abstract*— A coverage-based collaborative control strategy is developed in this paper for a multi-robot system with heterogeneous effective sensing ranges and safe operation zones to simultaneously estimate the states of and follow multiple targets governed by stochastic dynamics. Multiplicatively weighted Voronoi diagrams are exploited to define each robot's dominant region considering its limited sensing radius. The asymptotically stable system dynamics enabling the heterogeneous multi-robot system to (locally) optimally cover the time-varying probability density distributions that characterize the uncertainties of the targets' positions is derived, and minimally perturbed by control barrier functions designed to ensure that each robot moves within its safe operation zone in a collision-free manner. Specific target dynamics and measurement models are chosen in the experiment, whose results demonstrate the effectiveness of the proposed dynamic multi-target tracking approach.**

I. Introduction

Autonomous target tracking and following has a wide range of applications in both collaborative and adversarial scenarios, such as environmental monitoring, wildlife tracking, search and rescue, pursuit-evasion, and adversarial agent tracking and following [1]–[3]. The primary objective of target tracking is to estimate the states, e.g., positions, velocities, and accelerations, of targets of interest, as reviewed in [4]. For example, deploying a multi-robot team to track space-time dependent physical phenomena that may be harmful to human beings, such as pollution sources [5], radioactive wastes [6], and tornadoes [7].

Heterogeneous multi-robot systems are desired to collaboratively, efficiently, and robustly accomplish missions such as target tracking in complex and dynamic environments since it is burdensome for a single autonomous robot or a team of homogeneous robots to adapt to every potential circumstance, as discussed in [8]. Additionally, when the domain where targets of interest are moving is relatively large, it is more efficient to deploy mobile robots equipped with sensors that can dynamically track and follow the targets' motions rather than static robots because the larger the domain is, the more static robots need to be deployed in order to achieve certain task requirements, e.g., [9].

In [9], an optimal trajectory planning method is proposed for target tracking tasks using multiple sensors with a mixture of different measurement models, but the method can be only used to track a single moving target. A Voronoi-based joint optimization approach is introduced in [10] for a team of homogeneous sensors to cover the environment while estimating the states of multiple targets, but the probability density distributions characterizing the uncertainties of the targets' states are not considered in the process of sensors' coverage in that work. In addition, in [11], the problem of simultaneous coverage and multi-target tracking is solved based on mixed-integer programming with quadratic constraint, but the strategy is only suitable for the case of a single robot (tracker), although the robot is equipped with two types of sensors.

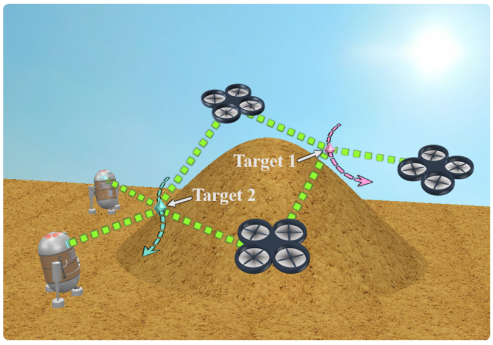

Fig. 1. Illustrating a multi-robot multi-target tracking scenario at a time moment: Two ground robots (left), whose safe operation zones are the domain excluding the hill, are dynamically tracking Target 2 while taking measurements of it, and three aerial robots (middle and right), whose safe operation zones are the entire domain of interest, are dynamically tracking Target 1 and Target 2 while taking measurements of them. The dashed lines with arrows represent the past and possible future trajectories of the targets with corresponding colors, and the dashed green lines reveal which robots can take measurements of which targets.

The main novelty of this paper is to propose a coverage-based heterogeneous multi-robot collaborative control strategy for simultaneous multi-target tracking and following, where the heterogeneities consist of: 1) The robots have heterogeneous perception characteristics, reflected by their different sensing radii; 2) When a target is located within any robots' effective sensing ranges and have the same distances to these robots, the measurement noises of the target taken by different robots are nonidentical; 3) The robots have heterogeneous mobility characteristics, reflected by their various safe operation zones, for example, when a multi-robot team consisting of aerial robots and ground robots is collaboratively tracking dynamic targets moving in a domain composed of flat lands and terrains with hills or bumps, aerial robots can fly over those terrains while ground robots are constrained in the flat lands, as illustrated in Fig. 1.

The motivation of the consideration of these heterogeneous modalities presented above is that heterogeneous robots can collaborate with each other on tasks that can not be accomplished by a single robot or a team of homogeneous

This work was supported by the U.S. Army Research Lab through ARL DCIST CRA W911NF-17-2-0181.

†Ruoyu Lin and Magnus Egerstedt are with the Department of Electrical Engineering and Computer Science, University of California, Irvine, CA 92697, USA. Email: {rlin10, magnus}@uci.edu

2023 IEEE/RSJ International Conference on Intelligent Robots and Systems (IROS) | 978-1-6654-9190-7/23/$31.00 ©2023 IEEE | DOI: 10.1109/IROS55552.2023.10342237

robots effectively, efficiently, or robustly. For instance, a) For tasks carried out by aerial robots and underwater robots in collaboration, although underwater robots are constrained in the water, they can take more accurate measurements underwater using sophisticated sonar sensors than aerial robots that have larger operation zones; b) The sensors installed on certain robots may have disadvantages of less sensing ranges but advantages of lower sensor noise intensities when taking measurements than other sensors; c) The robots with relatively smaller sensing ranges and higher noisy intensities may have lower power consumption and thus have longer operation duration compared to other robots.

This paper's remaining part is structured as follows: In Section II, the stochastic system dynamics of targets and measurement models of robots are briefly introduced. The control barrier certificates are presented in Section III to be employed to ensure that each robot in a multi-robot system moves only in its safe operation zone and does not collide with any other robots. In Section IV, the heterogeneous region of dominance of each robot according to its limited sensing range is defined and the resulting heterogeneous dynamics of the multi-robot system is derived for multi-target tracking tasks. Experimental results and conclusions are presented in Section V and Section VI, respectively.

II. Stochastic Models of Targets

Consider a team of N_s mobile robots to be deployed in a convex domain of interest $\mathcal{D} \subset \mathbb{R}^2$ to track N_t targets while taking measurements of them. Each robot is equipped with a sensory system with a particular sensing radius, and its position is assumed to be known by its neighboring (in the sense of Delaunay neighbors which will be discussed in detail in Section IV) robots. Denote the set of targets' indices as $\mathcal{N}_t = \{1, 2, \ldots, N_t\}$, the set of robots' indices as $\mathcal{N}_s = \{1, 2, \ldots, N_s\}$, where $N_t, N_s \in \mathbb{Z}^+$, the position of Target n, where $n \in \mathcal{N}_t$, at time t as $\boldsymbol{p}_{t,n}(t) \in \mathcal{D}$, and the position of Robot i, where $i \in \mathcal{N}_s$, at time t as $\boldsymbol{p}_{s,i}(t) \in \mathcal{D}$. Let $\boldsymbol{p}_s(t) = [\boldsymbol{p}_{s,1}^T(t), \boldsymbol{p}_{s,2}^T(t), \ldots, \boldsymbol{p}_{s,N_s}^T(t)]^T \in \mathbb{R}^{2N_s}$ be the vector consisting of the N_s robots' positions at time t, $\boldsymbol{r}_s = [r_{s,1}, r_{s,2}, \ldots, r_{s,N_s}]^T \in \mathbb{R}^{N_s}$ be the vector of their corresponding sensing radii, where $r_{s,i} \in \mathbb{R}_{>0}$, $\forall i \in \mathcal{N}_s$.

Denote the discrete-time dynamics of Target n as

$$\boldsymbol{x}_{t,n}(k+1) = \boldsymbol{f}_{t,n}(\boldsymbol{x}_{t,n}(k), \boldsymbol{u}_{t,n}(k), \boldsymbol{\xi}_{t,n}(k)), \tag{1}$$

for all $n \in \mathcal{N}_t$, in which $\boldsymbol{x}_{t,n}(k) = [\boldsymbol{p}_{t,n}^T(k), \dot{\boldsymbol{p}}_{t,n}^T(k)]^T$ is the state of Target n at time step $t = kT$ consisting of the position part $\boldsymbol{p}_{t,n}(t)$ and the velocity part $\dot{\boldsymbol{p}}_{t,n}(t)$, where $k \in \mathbb{Z}^+$ and T is a constant sampling interval, $\boldsymbol{u}_{t,n}(k)$ denotes the control input at time step $t = kT$, the vector-valued function $\boldsymbol{f}_{t,n}$ represents Target n's dynamics, and $\boldsymbol{\xi}_{t,n}(k)$ stands for the process noise at time step $t = kT$ encoding the stochasticity of Target n's dynamics.

Denote the space–time dependent functions $f_{\boldsymbol{p}_{t,n}}^-(\boldsymbol{q}, t) : \mathcal{D} \times \mathbb{R}_{\geq 0} \to \mathbb{R}_{>0}$ and $f_{\boldsymbol{p}_{t,n}}^+(\boldsymbol{q}, t) : \mathcal{D} \times \mathbb{R}_{\geq 0} \to \mathbb{R}_{>0}$ as the prior and posterior probability density functions of the position part $\boldsymbol{p}_{t,n}(t)$ of the state of Target n respectively. The posterior probability $f_{\boldsymbol{p}_{t,n}}^+$ is obtained by fusing $f_{\boldsymbol{p}_{t,n}}^-$ with the measurements of Target n taken by certain robots, where the discrete-time measurement model is defined as

$$\boldsymbol{z}_{n,i}(k) = \boldsymbol{h}_{n,i}(\boldsymbol{x}_{t,n}(k), \boldsymbol{\zeta}_{n,i}(k)), \tag{2}$$

for all $n \in \mathcal{N}_t$, $i \in \mathcal{N}_s$ such that

$$\|\boldsymbol{p}_{t,n}(k) - \boldsymbol{p}_{s,i}(k)\| \leq r_{s,i}, \tag{3}$$

where $\boldsymbol{\zeta}_{n,i}(k)$ stands for the measurement noise at time step $t = kT$ encoding the stochasticity of the measurements of Target n taken by Robot i, and $r_{s,i} \in \mathbb{R}_{>0}$ is the effective sensing radius of Robot i.

Based on specific dynamics and measurement models, and task requirements, one can employ any feasible state estimation techniques, e.g., [12], to obtain $f_{\boldsymbol{p}_{t,n}}^+(\boldsymbol{q}, t)$.

III. Safety of Multi-Robot Systems

The safety of collaborative multi-robot systems working in the domain of interest $\mathcal{D}$ considered in this paper is two-fold: A) Each robot has a safe operation zone; B) Each robot should not collide with any other robots.

Assume the dynamics of Robot i is in control-affine form

$$\dot{\boldsymbol{p}}_{s,i} = \boldsymbol{f}_{s,i}(\boldsymbol{p}_{s,i}) + \boldsymbol{g}_{s,i}(\boldsymbol{p}_{s,i})\boldsymbol{u}_{s,i}, \ \ \forall i \in \mathcal{N}_s, \tag{4}$$

with the vector fields $\boldsymbol{f}_{s,i}(\cdot) : \mathcal{D} \to \mathbb{R}^2$ and $\boldsymbol{g}_{s,i}(\cdot) : \mathcal{D} \to \mathbb{R}^{2\times m}$ both locally Lipschitz continuous, where $\boldsymbol{u}_{s,i} \in U_{s,i} \subset \mathbb{R}^m$ is an admissible control input for Robot i. Denote $\boldsymbol{p}_{s,ij} = [\boldsymbol{p}_{s,i}^T, \boldsymbol{p}_{s,j}^T]^T$ and $\boldsymbol{u}_{s,ij} = [\boldsymbol{u}_{s,i}^T, \boldsymbol{u}_{s,j}^T]^T \in U_{s,ij} \subset \mathbb{R}^{2m}$, $\forall i \neq j$, $i, j \in \mathcal{N}_s$, then

$$\dot{\boldsymbol{p}}_{s,ij} = \boldsymbol{f}_{s,ij}(\boldsymbol{p}_{s,ij}) + \boldsymbol{g}_{s,ij}(\boldsymbol{p}_{s,ij})\boldsymbol{u}_{s,ij}, \tag{5}$$

where $\boldsymbol{f}_{s,ij}(\cdot) : \mathcal{D}\times\mathcal{D} \to \mathbb{R}^4$ and $\boldsymbol{g}_{s,ij}(\cdot) : \mathcal{D}\times\mathcal{D} \to \mathbb{R}^{4\times 2m}$ are locally Lipschitz continuous vector fields.

Define the safe operation zone for Robot i as

$$\mathcal{A}_{s,i}(\boldsymbol{p}_{s,i}) = \left\{\boldsymbol{p}_{s,i} \in \mathcal{D} \,\middle|\, \hbar_{s,i}^A(\boldsymbol{p}_{s,i}) \geq 0\right\}, \tag{6}$$

where $\hbar_{s,i}^A(\cdot) : \mathcal{D} \to \mathbb{R}$ is continuously differentiable.

Define the collision-free set for the multi-robot team as

$$\mathcal{B}_{s,ij}(\boldsymbol{p}_{s,ij}) = \left\{\boldsymbol{p}_{s,ij} \in \mathcal{D}\times\mathcal{D} \,\middle|\, \hbar_{s,ij}^B(\boldsymbol{p}_{s,ij}) \geq 0\right\}, \tag{7}$$

where the continuously differentiable function $\hbar_{s,ij}^B(\cdot) : \mathcal{D}\times\mathcal{D} \to \mathbb{R}$ is specified as

$$\hbar_{s,ij}^B(\boldsymbol{p}_{s,ij}) = \|\boldsymbol{p}_{s,i} - \boldsymbol{p}_{s,j}\|^2 - D_{s,ij}^2, \tag{8}$$

where $D_{s,ij}$ is the safe distance between Robots i and j.

The functions $\hbar_{s,i}^A(\boldsymbol{p}_{s,i})$ and $\hbar_{s,ij}^B(\boldsymbol{p}_{s,ij})$ are said to be control barrier functions, e.g., [13], if there exists extended class $\mathcal{K}_\infty$ functions $\alpha(\cdot) : \mathbb{R} \to \mathbb{R}$ and $\beta(\cdot) : \mathbb{R} \to \mathbb{R}$ such that for the systems (4) and (5),

$$\sup_{\boldsymbol{u}_{s,i} \in U_{s,i}} \mathscr{C}_{s,i}^A(\boldsymbol{p}_{s,i}, \boldsymbol{u}_{s,i}) \geq 0, \tag{9}$$

and

$$\sup_{\boldsymbol{u}_{s,ij} \in U_{s,ij}} \mathscr{C}_{s,ij}^B(\boldsymbol{p}_{s,ij}, \boldsymbol{u}_{s,ij}) \geq 0, \tag{10}$$

respectively, where

$$\mathscr{C}^A_{s,i}(\boldsymbol{p}_{s,i},\boldsymbol{u}_{s,i}) = \mathcal{L}_{\boldsymbol{f}_{s,i}}\hbar^A_{s,i}(\boldsymbol{p}_{s,i}) + \mathcal{L}_{\boldsymbol{g}_{s,i}}\hbar^A_{s,i}(\boldsymbol{p}_{s,i})\boldsymbol{u}_{s,i} + \alpha(\hbar^A_{s,i}(\boldsymbol{p}_{s,i})), \tag{11}$$

and

$$\mathscr{C}^B_{s,ij}(\boldsymbol{p}_{s,ij},\boldsymbol{u}_{s,ij}) = \mathcal{L}_{\boldsymbol{f}_{s,ij}}\hbar^B_{s,ij}(\boldsymbol{p}_{s,ij}) + \mathcal{L}_{\boldsymbol{g}_{s,ij}}\hbar^B_{s,ij}(\boldsymbol{p}_{s,ij})\boldsymbol{u}_{s,ij} + \beta(\hbar^B_{s,ij}(\boldsymbol{p}_{s,ij})), \tag{12}$$

in which $\mathcal{L}$ stands for the Lie derivative. The corresponding safe control sets are

$$\mathcal{U}_{s,i}(\boldsymbol{p}_{s,i}) = \left\{\boldsymbol{u}_{s,i} \in U_{s,i} \,\middle|\, \mathscr{C}^A_{s,i}(\boldsymbol{p}_{s,i},\boldsymbol{u}_{s,i}) \geq 0\right\}, \tag{13}$$

and

$$\mathcal{U}_{s,ij}(\boldsymbol{p}_{s,ij}) = \left\{\boldsymbol{u}_{s,ij} \in U_{s,ij} \,\middle|\, \mathscr{C}^B_{s,ij}(\boldsymbol{p}_{s,ij},\boldsymbol{u}_{s,ij}) \geq 0\right\}, \tag{14}$$

respectively.

However, the nominal control inputs $\boldsymbol{u}_{s,i}$ and $\boldsymbol{u}_{s,ij}$ may not belong to $\mathcal{U}_{s,i}(\boldsymbol{p}_{s,i})$ defined in (13) and $\mathcal{U}_{s,ij}(\boldsymbol{p}_{s,ij})$ defined in (14) respectively, in which situation the actual control input $\hat{\boldsymbol{u}}_{s,i}$, $\forall i \in \mathcal{N}_s$, can be obtained in a minimally perturbed manner while ensuring safety by, e.g., [13],

$$\begin{aligned} \min_{\hat{\boldsymbol{u}}_s \in \mathcal{U}_s} \ & \|\hat{\boldsymbol{u}}_s - \boldsymbol{u}_s\|^2 \\ \text{s.t.} \ & \mathscr{C}^A_{s,i}(\boldsymbol{p}_{s,i},\hat{\boldsymbol{u}}_{s,i}) \geq 0, \quad \forall\, i \in \mathcal{N}_s \\ & \mathscr{C}^B_{s,ij}(\boldsymbol{p}_{s,ij},\hat{\boldsymbol{u}}_{s,ij}) \geq 0, \quad \forall\, i \neq j,\, i,j \in \mathcal{N}_s, \end{aligned} \tag{15}$$

where $\hat{\boldsymbol{u}}_s = [\hat{\boldsymbol{u}}^T_{s,1}, \hat{\boldsymbol{u}}^T_{s,2}, \ldots, \hat{\boldsymbol{u}}^T_{s,N_s}]^T \in U_s \subset \mathbb{R}^{mN_s}$, $\boldsymbol{u}_s = [\boldsymbol{u}^T_{s,1}, \boldsymbol{u}^T_{s,2}, \ldots, \boldsymbol{u}^T_{s,N_s}]^T \in U_s \subset \mathbb{R}^{mN_s}$, and $\hat{\boldsymbol{u}}_{s,ij} = [\hat{\boldsymbol{u}}^T_{s,i}, \hat{\boldsymbol{u}}^T_{s,j}]^T \in U_{s,ij} \subset \mathbb{R}^{2m}$.

Note that in [14], the concept of mobility-based operating regions is formulated similarly as (6) and (9), whereas the difference between it and the concept of safe operation zones formulated in this paper is that the safe operation zones we defined in this paper are assumed to not affect the dominant region partitioning among robots, which will be discussed in detail in Section IV, because the tasks of robots in this paper is to take measurements of targets through remote sensors, rather than to physically visit locations for event services.

IV. Heterogeneous Multi-Robot System Dynamics for Multi-Target Tracking

In this section, we investigate the nominal system dynamics (which needs to be perturbed in a minimally invasive manner to ensure the safety of the robots using the method proposed in Section III) of a multi-robot team for the task of multi-target tracking based on the assumption of heterogeneous sensing radii of robots.

Suppose the larger effective sensing radius a robot has, the larger region of dominance the robot should have. Therefore, analogous to [15], we assign the robots with multiplicatively weighted Voronoi cells (consisting of Apollonian circles) as their regions of dominance, and the weighting factors are assumed to have positive linear correlations with their sensing radii $r_{s,i}$, $\forall i \in \mathcal{N}_s$. Specifically, the dominant region of Robot i at time t is defined as

$$\mathcal{S}_i(\boldsymbol{p}_s) = \left\{\boldsymbol{q} \in \mathcal{D} \,\middle|\, \frac{\|\boldsymbol{p}_{s,i}(t) - \boldsymbol{q}\|}{f_{pc}(r_{s,i})} \leq \frac{\|\boldsymbol{p}_{s,j}(t) - \boldsymbol{q}\|}{f_{pc}(r_{s,j})}, \forall j\right\}, \tag{16}$$

where $j \neq i$, $i,j \in \mathcal{N}_s$, and $f_{pc}(\cdot) : \mathbb{R}_{>0} \to \mathbb{R}_{>0}$ is a positive linear correlation mapping, i.e., $f_{pc}(z) = k_{pc} \cdot z$, where $z, k_{pc} \in \mathbb{R}_{>0}$. According to [15], it can be shown that if Target $n, \forall n \in \mathcal{N}_t$ in the dominant region of Robot i at time t is not located within the sensing radius of Robot i, then Target n is not located within the sensing radius of Robot j, $\forall j \neq i, i,j \in \mathcal{N}_s$, as illustrated in Fig. 2.

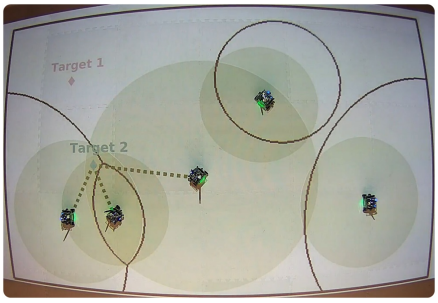

Fig. 2. Each robot has a region of dominance, i.e., a multiplicatively weighted Voronoi cell, with a set of black curves as its boundary, and an effective sensing circular region represented by a green circle. Target 1 is within no robot's effective sensing range, while Target 2 is within three robots' effective sensing ranges.

Since the true positions of the targets are unknown to the robots, we want the robots to optimally cover the probability density distributions characterizing the uncertainties of the targets' positions to increase the robots' chances of detecting the targets considering their heterogeneous effective sensing radii, resulting in more robots in the area (with a given Lebesgue measure) in which the targets are more likely to show up, where the optimality is in terms of the cost function that will be defined below. Assuming the coverage quality of a point $\boldsymbol{q} \in \mathcal{D}$ by Robot i at the position $\boldsymbol{p}_{s,i}(t)$ degrades with the weighted distance $\|\boldsymbol{p}_{s,i}(t) - \boldsymbol{q}\|/f_{pc}(r_{s,i})$ between $\boldsymbol{p}_{s,i}(t)$ and $\boldsymbol{q}$, the cost function encoding the lack of coverage quality over $\mathcal{D}$ can be defined as

$$C(\boldsymbol{p}_s,t) = \sum_{i\in\mathcal{N}_s} \int_{\mathcal{S}_i(\boldsymbol{p}_s)} \frac{\|\boldsymbol{p}_{s,i}(t) - \boldsymbol{q}\|^2}{f^2_{pc}(r_{s,i})} \sum_{n\in\mathcal{N}_t} f^+_{\boldsymbol{p}_{t,n}}(\boldsymbol{q},t)\, d\boldsymbol{q}. \tag{17}$$

Similar to [16], [17], we rewrite (17) as a summation of three terms $C(\boldsymbol{p}_s,t) = C_1(\boldsymbol{p}_s,t) + C_2(\boldsymbol{p}_s,t) + C_3(\boldsymbol{p}_s,t)$, where

$$C_1(\boldsymbol{p}_s,t) = \int_{\mathcal{S}_i(\boldsymbol{p}_s)} \frac{\|\boldsymbol{p}_{s,i}(t) - \boldsymbol{q}\|^2}{f^2_{pc}(r_{s,i})} \sum_{n\in\mathcal{N}_t} f^+_{\boldsymbol{p}_{t,n}}(\boldsymbol{q},t)\, d\boldsymbol{q},$$

$$C_2(\boldsymbol{p}_s,t) = \sum_{j\in\mathcal{N}_{\mathcal{S}_i}} \int_{\mathcal{S}_j(\boldsymbol{p}_s)} \frac{\|\boldsymbol{p}_{s,j}(t) - \boldsymbol{q}\|^2}{f^2_{pc}(r_{s,j})} \sum_{n\in\mathcal{N}_t} f^+_{\boldsymbol{p}_{t,n}}(\boldsymbol{q},t)\, d\boldsymbol{q},$$

and

$$C_3(\boldsymbol{p}_s,t) = \sum_{j\notin\overline{\mathcal{N}_{\mathcal{S}_i}}} \int_{\mathcal{S}_j(\boldsymbol{p}_s)} \frac{\|\boldsymbol{p}_{s,j}(t) - \boldsymbol{q}\|^2}{f^2_{pc}(r_{s,j})} \sum_{n\in\mathcal{N}_t} f^+_{\boldsymbol{p}_{t,n}}(\boldsymbol{q},t)\, d\boldsymbol{q},$$

where $\mathcal{N}_{\mathcal{S}_i}$ and $\overline{\mathcal{N}_{\mathcal{S}}}_i$ stand for the set of indices of Delaunay neighbors of Robot i and the set of indices of the closed neighborhood of Robot i in the Delaunay graph, respectively.

Lemma 1: (Leibniz Integral Rule, e.g., [18]) For the function

$$F(\boldsymbol{p},t)=\int_{\Omega(\boldsymbol{p})} f(\boldsymbol{p},t,\boldsymbol{q})\,d\boldsymbol{q},$$

where $f(\boldsymbol{p},t,\boldsymbol{q}):\mathbb{R}^{2N_s}\times\mathbb{R}_{\geq 0}\times\mathbb{R}^2\to\mathbb{R}$, and $\Omega(\boldsymbol{p})\subset\mathbb{R}^2$ depends smoothly on $\boldsymbol{p}$,

$$\frac{\partial F(\boldsymbol{p},t)}{\partial \boldsymbol{p}}=\int_{\Omega(\boldsymbol{p})}\frac{\partial f(\boldsymbol{p},t,\boldsymbol{q})}{\partial \boldsymbol{p}}d\boldsymbol{q}+\int_{\partial\Omega(\boldsymbol{p})} f(\boldsymbol{p},t,\boldsymbol{q})\bar{\boldsymbol{n}}_{\partial\Omega}^T\frac{\partial \boldsymbol{q}_{\partial\Omega}}{\partial \boldsymbol{p}}d\boldsymbol{q},$$

where $\boldsymbol{q}_{\partial\Omega}$ denotes a point on $\partial\Omega$, and $\bar{\boldsymbol{n}}_{\partial\Omega}$ denotes an outward-pointing unit normal uniquely defined at almost every $\boldsymbol{q}_{\partial\Omega}$.

Proof: See [18]. □

Utilizing Lemma 1, we have

$$\begin{aligned}\frac{\partial C_1(\boldsymbol{p}_s,t)}{\partial \boldsymbol{p}_{s,i}}=&\int_{\mathcal{S}_i(\boldsymbol{p}_s)}\frac{\sum_{n\in\mathcal{N}_t}2f^+_{\boldsymbol{p}_{t,n}}(\boldsymbol{q},t)}{f^2_{pc}(r_{s,i})}(\boldsymbol{p}_{s,i}-\boldsymbol{q})^T\,d\boldsymbol{q}\\&+\sum_{j\in\mathcal{N}_{\mathcal{S}_i}}\int_{\partial\mathcal{S}_{ij}(\boldsymbol{p}_s)}\frac{\|\boldsymbol{p}_{s,i}(t)-\boldsymbol{q}\|^2}{f^2_{pc}(r_{s,i})}\cdot\\&\sum_{n\in\mathcal{N}_t}f^+_{\boldsymbol{p}_{t,n}}(\boldsymbol{q},t)\,\bar{\boldsymbol{n}}^T_{\partial\mathcal{S}_{ij}}(\boldsymbol{q})\frac{\partial \boldsymbol{q}_{\partial\mathcal{S}_{ij}}(\boldsymbol{p}_s)}{\partial \boldsymbol{p}_{s,i}}\,d\boldsymbol{q},\end{aligned}\tag{18}$$

where $\partial\mathcal{S}_{ij}(\boldsymbol{p}_s)$, $\boldsymbol{q}_{\partial\mathcal{S}_{ij}}(\boldsymbol{p}_s)$, and $\bar{\boldsymbol{n}}_{\partial\mathcal{S}_{ij}}(\boldsymbol{q})$ denote the boundary shared by the dominant regions of Robot i and Robot j, a point on $\partial\mathcal{S}_{ij}(\boldsymbol{p}_s)$, and the unit outward normal on $\partial\mathcal{S}_{ij}(\boldsymbol{p}_s)$ pointing from $\boldsymbol{p}_{s,i}$ to $\boldsymbol{p}_{s,j}$, respectively.

Note that only $\boldsymbol{q}_{\partial\mathcal{S}_{ij}}(\boldsymbol{p}_s)$ is left in (18) as the integration variable because the partial derivative of any point in any subset of the boundary of the dominant region of Robot i that coincide with the boundary of $\mathcal{D}$ with respect to $\boldsymbol{p}_{s,i}$ is zero. Likewise,

$$\begin{aligned}\frac{\partial C_2(\boldsymbol{p}_s,t)}{\partial \boldsymbol{p}_{s,i}}=&-\sum_{j\in\mathcal{N}_{\mathcal{S}_i}}\int_{\partial\mathcal{S}_{ij}(\boldsymbol{p}_s)}\frac{\|\boldsymbol{p}_{s,j}(t)-\boldsymbol{q}\|^2}{f^2_{pc}(r_{s,j})}\cdot\\&\sum_{n\in\mathcal{N}_t}f^+_{\boldsymbol{p}_{t,n}}(\boldsymbol{q},t)\,\bar{\boldsymbol{n}}^T_{\partial\mathcal{S}_{ij}}(\boldsymbol{q})\frac{\partial \boldsymbol{q}_{\partial\mathcal{S}_{ij}}(\boldsymbol{p}_s)}{\partial \boldsymbol{p}_{s,i}}\,d\boldsymbol{q},\end{aligned}\tag{19}$$

and

$$\frac{\partial C_3(\boldsymbol{p}_s,t)}{\partial \boldsymbol{p}_{s,i}}=0.\tag{20}$$

As such, according to the property of $\partial\mathcal{S}_{ij}(\boldsymbol{p}_s)$,

$$\frac{\partial C(\boldsymbol{p}_s,t)}{\partial \boldsymbol{p}_{s,i}}=\int_{\mathcal{S}_i(\boldsymbol{p}_s)}\frac{\sum_{n\in\mathcal{N}_t}2f^+_{\boldsymbol{p}_{t,n}}(\boldsymbol{q},t)}{f^2_{pc}(r_{s,i})}(\boldsymbol{p}_{s,i}-\boldsymbol{q})^T\,d\boldsymbol{q}.\tag{21}$$

Define the mass $m_{s,i}(\boldsymbol{p}_s,t)$ and center of mass $\boldsymbol{c}_{s,i}(\boldsymbol{p}_s,t)$ of the dominant region of Robot i as

$$m_{s,i}(\boldsymbol{p}_s,t)=\int_{\mathcal{S}_i(\boldsymbol{p}_s)}\sum_{n\in\mathcal{N}_t}f^+_{\boldsymbol{p}_{t,n}}(\boldsymbol{q},t)\,d\boldsymbol{q}\tag{22}$$

and

$$\boldsymbol{c}_{s,i}(\boldsymbol{p}_s,t)=\frac{\int_{\mathcal{S}_i(\boldsymbol{p}_s)}\boldsymbol{q}\sum_{n\in\mathcal{N}_t}f^+_{\boldsymbol{p}_{t,n}}(\boldsymbol{q},t)\,d\boldsymbol{q}}{m_{s,i}(\boldsymbol{p}_s,t)}\tag{23}$$

respectively. Then (21) can be rewritten as

$$\frac{\partial C(\boldsymbol{p}_s,t)}{\partial \boldsymbol{p}_{s,i}}=\frac{2m_{s,i}(\boldsymbol{p}_s,t)}{f^2_{pc}(r_{s,i})}(\boldsymbol{p}_{s,i}(t)-\boldsymbol{c}_{s,i}(\boldsymbol{p}_s,t))^T,\tag{24}$$

which implies that a critical point of (17) with respect to $\boldsymbol{p}_{s,i}$, $\forall i\in\mathcal{N}_s$ is

$$\boldsymbol{p}^*_{s,i}(t)=\boldsymbol{c}_{s,i}(\boldsymbol{p}_s,t).\tag{25}$$

Note that the requirement of $f^+_{\boldsymbol{p}_{t,n}}(\boldsymbol{q},t)\in\mathbb{R}_{>0}$, $\forall n\in\mathcal{N}_t$, presented in Section II can be relaxed to $m_{s,i}(\boldsymbol{p}_s,t)\in\mathbb{R}_{>0}$, $\forall i\in\mathcal{N}_s$, as long as (23) is well-defined.

In order to find out a system dynamics of the heterogeneous multi-robot team to achieve and maintain the critical point (25) for all $i\in\mathcal{N}_s$, we analyze the Lyapunov function

$$V(\boldsymbol{p}_s,t)=\frac{1}{2}\sum_{i\in\mathcal{N}_s}\|\boldsymbol{p}_{s,i}(t)-\boldsymbol{c}_{s,i}(\boldsymbol{p}_s,t)\|^2,\tag{26}$$

whose time derivative is (some explicit dependencies of the variables will be dropped for notational convenience in the following content)

$$\dot{V}=(\boldsymbol{p}_s-\boldsymbol{c}_s)^T\left(\left(I-\frac{\partial \boldsymbol{c}_s}{\partial \boldsymbol{p}_s}\right)\dot{\boldsymbol{p}}_s-\frac{\partial \boldsymbol{c}_s}{\partial t}\right),\tag{27}$$

where $\boldsymbol{c}_s(\boldsymbol{p}_s,t)=[\boldsymbol{c}^T_{s,1}(\boldsymbol{p}_s,t),\ldots,\boldsymbol{c}^T_{s,N_s}(\boldsymbol{p}_s,t)]^T\in\mathbb{R}^{2N_s}$, and I is an identity matrix with the corresponding dimension. Analogous to [19], one way to enforce (27) to be negative definite is to let

$$\dot{\boldsymbol{p}}_s=\left(I-\frac{\partial \boldsymbol{c}_s}{\partial \boldsymbol{p}_s}\right)^{-1}\left(\kappa\,(\boldsymbol{c}_s-\boldsymbol{p}_s)+\frac{\partial \boldsymbol{c}_s}{\partial t}\right),\tag{28}$$

where $\kappa\in\mathbb{R}_{>0}$, and

$$\frac{\partial \boldsymbol{c}_s}{\partial \boldsymbol{p}_s}=\begin{pmatrix}\frac{\partial \boldsymbol{c}_{s,1}}{\partial \boldsymbol{p}_{s,1}}&\cdots&\frac{\partial \boldsymbol{c}_{s,1}}{\partial \boldsymbol{p}_{s,N_s}}\\\vdots&\ddots&\vdots\\\frac{\partial \boldsymbol{c}_{s,N_s}}{\partial \boldsymbol{p}_{s,1}}&\cdots&\frac{\partial \boldsymbol{c}_{s,N_s}}{\partial \boldsymbol{p}_{s,N_s}}\end{pmatrix}\in\mathbb{R}^{2N_s\times 2N_s}.\tag{29}$$

Therefore, as long as the inverse term in (28) is well-defined, $\boldsymbol{p}_s(t)$ governed by (28) converges to $\boldsymbol{c}_s(\boldsymbol{p}_s,t)$ as $t\to\infty$ with the exponential convergence rate $exp(-2\kappa t)$.

Lemma 2: The shared boundary of the dominant regions of Robots i and j is given by the Apollonius circle, e.g., [20]

$$\partial\mathcal{S}_{ij}=\left\{\boldsymbol{q}\in\mathcal{D}\,\middle|\,\|\boldsymbol{q}-\boldsymbol{c}_{Ap,ij}\|=r_{Ap,ij}\right\},\tag{30}$$

where

$$\boldsymbol{c}_{Ap,ij}=\frac{f^2_{pc}(r_{s,j})\boldsymbol{p}_{s,i}-f^2_{pc}(r_{s,i})\boldsymbol{p}_{s,j}}{f^2_{pc}(r_{s,j})-f^2_{pc}(r_{s,i})}$$

and

$$r_{Ap,ij}=\frac{f_{pc}(r_{s,i})f_{pc}(r_{s,j})\|\boldsymbol{p}_{s,i}-\boldsymbol{p}_{s,j}\|}{f^2_{pc}(r_{s,j})-f^2_{pc}(r_{s,i})},$$

where $f_{pc}(r_{s,i})<f_{pc}(r_{s,j})$. When $f_{pc}(r_{s,i})=f_{pc}(r_{s,j})$, $\partial\mathcal{S}_{ij}$ becomes a straight line, i.e., the radius of the corresponding Apollonius circle becomes infinite.

Proof: Squaring both sides of the equation defined as (16) with the inequality replaced by equality yields

$$f^2_{pc}(r_{s,j})(\boldsymbol{q}-\boldsymbol{p}_{s,i})^2=f^2_{pc}(r_{s,i})(\boldsymbol{q}-\boldsymbol{p}_{s,j})^2,\tag{31}$$

where we define $\boldsymbol{z}^2 := \boldsymbol{z}^T\boldsymbol{z}$, $\forall \boldsymbol{z} \in \mathbb{R}^2$. Manipulating (31) yields

$$f_{pc}^2(r_{s,i})\boldsymbol{p}_{s,j}^2 - f_{pc}^2(r_{s,j})\boldsymbol{p}_{s,i}^2 = (f_{pc}^2(r_{s,j}) - f_{pc}^2(r_{s,i}))\boldsymbol{q}^2 - 2\boldsymbol{q}^T(f_{pc}^2(r_{s,j})\boldsymbol{p}_{s,i} - f_{pc}^2(r_{s,i})\boldsymbol{p}_{s,j}). \quad (32)$$

Multiplying both sides of (32) by $(f_{pc}^2(r_{s,j}) - f_{pc}^2(r_{s,i}))$ yields

$$f_{pc}^2(r_{s,i})(f_{pc}^2(r_{s,j}) - f_{pc}^2(r_{s,i}))\boldsymbol{p}_{s,j}^2 - f_{pc}^2(r_{s,j})(f_{pc}^2(r_{s,j}) - f_{pc}^2(r_{s,i}))\boldsymbol{p}_{s,i}^2 = (f_{pc}^2(r_{s,j}) - f_{pc}^2(r_{s,i}))^2\boldsymbol{q}^2 - 2\boldsymbol{q}^T (f_{pc}^2(r_{s,j}) - f_{pc}^2(r_{s,i}))(f_{pc}^2(r_{s,j})\boldsymbol{p}_{s,i} - f_{pc}^2(r_{s,i})\boldsymbol{p}_{s,j}). \quad (33)$$

Manipulating (33) yields

$$\frac{f_{pc}^2(r_{s,i})f_{pc}^2(r_{s,j})(\boldsymbol{p}_{s,i} - \boldsymbol{p}_{s,j})^2}{(f_{pc}^2(r_{s,j}) - f_{pc}^2(r_{s,i}))^2} = \boldsymbol{q}^2 - 2\boldsymbol{q}^T \frac{f_{pc}^2(r_{s,j})\boldsymbol{p}_{s,i} - f_{pc}^2(r_{s,i})\boldsymbol{p}_{s,j}}{f_{pc}^2(r_{s,j}) - f_{pc}^2(r_{s,i})} + \frac{(f_{pc}^2(r_{s,j})\boldsymbol{p}_{s,i} - f_{pc}^2(r_{s,i})\boldsymbol{p}_{s,j})^2}{(f_{pc}^2(r_{s,j}) - f_{pc}^2(r_{s,i}))^2}. \quad (34)$$

Taking square root on both sides of (34) yields (30). When $f_{pc}(r_{s,i}) = f_{pc}(r_{s,j})$, one can see from (31) that $\partial\mathcal{S}_{ij}$ becomes the perpendicular bisector of the line segment with $\boldsymbol{p}_{s,i}$ and $\boldsymbol{p}_{s,j}$ as the two endpoints. □

Utilizing Lemma 1 and Lemma 2, and based on (22) and (23), the partial derivative $\frac{\partial \boldsymbol{c}_{s,i}}{\partial \boldsymbol{p}_{s,i}}$ in (28) and (29) can be calculated as

$$\frac{\partial \boldsymbol{c}_{s,i}}{\partial \boldsymbol{p}_{s,i}} = \frac{1}{m_{s,i}} \sum_{k\in\mathcal{N}_{\mathcal{S}_i}} \int_{\partial\mathcal{S}_{ik}} \frac{\boldsymbol{q}\sum_{n\in\mathcal{N}_t} f_{\boldsymbol{p}_{t,n}}^+(\boldsymbol{q},t)(\boldsymbol{q}-\boldsymbol{p}_{s,i})^T}{f_{pc}^2(r_{s,i})\left\|\frac{\boldsymbol{q}-\boldsymbol{p}_{s,i}}{f_{pc}^2(r_{s,i})} - \frac{\boldsymbol{q}-\boldsymbol{p}_{s,k}}{f_{pc}^2(r_{s,k})}\right\|} d\boldsymbol{q} - \frac{\boldsymbol{c}_{s,i}}{m_{s,i}} \sum_{k\in\mathcal{N}_{\mathcal{S}_i}} \int_{\partial\mathcal{S}_{ik}} \frac{\sum_{n\in\mathcal{N}_t} f_{\boldsymbol{p}_{t,n}}^+(\boldsymbol{q},t)(\boldsymbol{q}-\boldsymbol{p}_{s,i})^T}{f_{pc}^2(r_{s,i})\left\|\frac{\boldsymbol{q}-\boldsymbol{p}_{s,i}}{f_{pc}^2(r_{s,i})} - \frac{\boldsymbol{q}-\boldsymbol{p}_{s,k}}{f_{pc}^2(r_{s,k})}\right\|} d\boldsymbol{q}. \quad (35)$$

Likewise, $\frac{\partial \boldsymbol{c}_{s,i}}{\partial \boldsymbol{p}_{s,j}}$ can be calculated as

$$\frac{\partial \boldsymbol{c}_{s,i}}{\partial \boldsymbol{p}_{s,j}} = \frac{-1}{m_{s,i}} \int_{\partial\mathcal{S}_{ij}} \frac{\boldsymbol{q}\sum_{n\in\mathcal{N}_t} f_{\boldsymbol{p}_{t,n}}^+(\boldsymbol{q},t)(\boldsymbol{q}-\boldsymbol{p}_{s,j})^T}{f_{pc}^2(r_{s,j})\left\|\frac{\boldsymbol{q}-\boldsymbol{p}_{s,j}}{f_{pc}^2(r_{s,j})} - \frac{\boldsymbol{q}-\boldsymbol{p}_{s,i}}{f_{pc}^2(r_{s,i})}\right\|} d\boldsymbol{q} + \frac{\boldsymbol{c}_{s,i}}{m_{s,i}} \int_{\partial\mathcal{S}_{ij}} \frac{\sum_{n\in\mathcal{N}_t} f_{\boldsymbol{p}_{t,n}}^+(\boldsymbol{q},t)(\boldsymbol{q}-\boldsymbol{p}_{s,j})^T}{f_{pc}^2(r_{s,j})\left\|\frac{\boldsymbol{q}-\boldsymbol{p}_{s,j}}{f_{pc}^2(r_{s,j})} - \frac{\boldsymbol{q}-\boldsymbol{p}_{s,i}}{f_{pc}^2(r_{s,i})}\right\|} d\boldsymbol{q}, \quad (36)$$

for all $j \in \mathcal{N}_{\mathcal{S}_i}$, and

$$\frac{\partial \boldsymbol{c}_{s,i}}{\partial \boldsymbol{p}_{s,j}} = 0, \quad (37)$$

for all $j \notin \overline{\mathcal{N}_{\mathcal{S}_i}}$. In addition, the time derivative of $\boldsymbol{c}_{s,i}$ can be calculated as

$$\frac{\partial \boldsymbol{c}_{s,i}}{\partial t} = \frac{1}{m_{s,i}} \int_{\mathcal{S}_i} (\boldsymbol{q} - \boldsymbol{c}_{s,i}) \frac{\partial}{\partial t} \sum_{n\in\mathcal{N}_t} f_{\boldsymbol{p}_{t,n}}^+(\boldsymbol{q},t)\, d\boldsymbol{q}. \quad (38)$$

In order to avoid the situation of nonexistence of the inverse term in (28), one can use the first $N_l + 1$ entries of the Neumann series, e.g., [19], of the inverse term in (28) to approximate (28) as

$$\dot{\boldsymbol{p}}_s = \sum_{l=0}^{N_l} \left(\frac{\partial \boldsymbol{c}_s}{\partial \boldsymbol{p}_s}\right)^l \left(\kappa(\boldsymbol{c}_s - \boldsymbol{p}_s) + \frac{\partial \boldsymbol{c}_s}{\partial t}\right). \quad (39)$$

The multi-robot system dynamics (39) drives a team of robots to optimally (in terms of (17)) cover the probability density distributions characterizing the uncertainties of the targets' positions. Meanwhile, the robots are taking measurements of the targets, based on which any feasible state estimation techniques can be applied to minimize the uncertainties of targets' states consisting of position parts and velocity parts.

V. Experiment

In this section, we implement the multi-target tracking strategy proposed in this paper on $N_t = 2$ targets and $N_s = 5$ differential-drive wheeled robots at the Robotarium [21], where $\mathcal{D}$ is a rectangular domain with x-axis ranging from -1.6 to 1.6, y-axis ranging from -1 to 1, and origin at the center. We assume the single integrator dynamics of $\boldsymbol{p}_s$ in (39) and $\boldsymbol{p}_s$ corresponds to points near off the axles of the wheels of the robots.

A. Targets' Dynamics and Measurement Models

Although the multi-target tracking strategy proposed in this paper can work for targets with any dynamics model (1) and measurement model (2) presented in Section II, we need to specify ones to demonstrate the proposed strategy in robotic experiments. Since studying state estimation techniques for general dynamics and measurement models is not the main point of this paper, we simply choose a linear dynamics with an additive white noise for the dynamics of a target. Specifically, we define the discrete-time dynamics of Target n as the coordinated turn model, e.g., [4]

$$\boldsymbol{x}_{t,n}(k+1) = F_{t,n}(\omega_{t,n})\boldsymbol{x}_{t,n}(k) + \boldsymbol{\xi}_{t,n}(k), \quad (40)$$

where $\omega_{t,n}$ is the turn rate, each entry of $F_{t,n}(\omega_{t,n}) \in \mathbb{R}^{4\times4}$ is defined as $F_{t,n}^{11} = F_{t,n}^{22} = 1$, $F_{t,n}^{12} = F_{t,n}^{21} = F_{t,n}^{31} = F_{t,n}^{32} = F_{t,n}^{41} = F_{t,n}^{42} = 0$, $F_{t,n}^{13} = F_{t,n}^{24} = \sin(\omega_{t,n}T)/\omega_{t,n}$, $F_{t,n}^{14} = -F_{t,n}^{23} = (\cos(\omega_{t,n}T) - 1)/\omega_{t,n}$, $F_{t,n}^{33} = F_{t,n}^{44} = \cos(\omega_{t,n}T)$, and $F_{t,n}^{43} = -F_{t,n}^{34} = \sin(\omega_{t,n}T)$, in which $F_{t,n}^{ab}$ stands for the element at a^{th} row and b^{th} column of $F_{t,n}$, T is a constant sampling interval, and $\boldsymbol{\xi}_{t,n}(k)$ is a discrete-time zero-mean white process noise of Target n, whose covariance is

$$Q_{t,n}(k) := \mathbb{E}[\boldsymbol{\xi}_{t,n}(k)\boldsymbol{\xi}_{t,n}^T(k)] = S_{\boldsymbol{\xi}_{t,n}} M_{t,n}, \quad (41)$$

where each entry of $M_{t,n} \in \mathbb{R}^{4\times4}$ is defined as $M_{t,n}^{11} = M_{t,n}^{22} = 2(\omega_{t,n}T - \sin(\omega_{t,n}T))/\omega_{t,n}^3$, $M_{t,n}^{12} = M_{t,n}^{21} = M_{t,n}^{34} = M_{t,n}^{43} = 0$, $M_{t,n}^{13} = M_{t,n}^{31} = M_{t,n}^{24} = M_{t,n}^{42} = (1 - \cos(\omega_{t,n}T))/\omega_{t,n}^2$, $M_{t,n}^{14} = M_{t,n}^{41} = -M_{t,n}^{23} = -M_{t,n}^{32} = (\omega_{t,n}T - \sin(\omega_{t,n}T))/\omega_{t,n}^2$, $M_{t,n}^{33} = M_{t,n}^{44} = T$, in which $M_{t,n}^{ab}$ represents the element at a^{th} row and b^{th} column of $M_{t,n}$, and $S_{\boldsymbol{\xi}_{t,n}}$ stands for the power spectral density of $\boldsymbol{\xi}_{t,n}$.

The discrete-time measurement model is defined as

$$\boldsymbol{z}_{n,i}(k) = H_{n,i}(k)\boldsymbol{x}_{t,n}(k) + \boldsymbol{\zeta}_{n,i}(k), \quad (42)$$

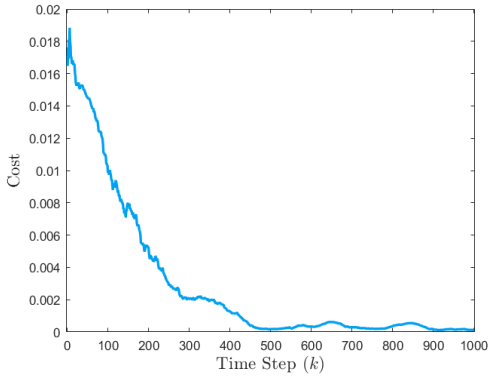

Fig. 3. Instantaneous cost $C(\boldsymbol{p}_s, k)$ in (17) along time step k.

for all $n \in \mathcal{N}_t$ and $i \in \mathcal{N}_s$ such that $\|\boldsymbol{p}_{t,n}(k) - \boldsymbol{p}_{s,i}(k)\| \leq r_{s,i}$, where $H_{n,i}(k) \in \mathbb{R}^{4\times 4}$, $\boldsymbol{\zeta}_{n,i}(k)$ is the vector of a discrete-time zero-mean white noise sequence of the measurement of Target n taken by Robot i, whose covariance is defined as

$$R_{n,i}(k) := \mathbb{E}[\boldsymbol{\zeta}_{n,i}(k)\boldsymbol{\zeta}_{n,i}^T(k)] = \lambda_{n,i}(k)M_{n,i}(k), \qquad (43)$$

where $M_{n,i}^R(k)$ is a symmetric and positive semi-definite matrix, and $\lambda_{n,i}(k) := \eta_{n,i}\|\boldsymbol{p}_{t,n}(k) - \boldsymbol{p}_{s,i}(k)\| \in \mathbb{R}_{>0}$ reflects that the noise intensity of the measurement of Target n taken by Robot i is larger when Target n is farther from Robot i, and vice versa, where $\eta_{n,i} \in \mathbb{R}_{>0}$ encodes Heterogeneity 2) presented in Section I.

Now that the targets' system model and measurement model are both assumed linear and subject to zero-mean white Gaussian noise, we can employ the Kalman filter to recursively estimate the state of Target n as follows.

Prediction:

$$\boldsymbol{x}_{t,n}^-(k) = F_{t,n}(\omega_{t,n})\boldsymbol{x}_{t,n}^+(k-1),$$
$$P_{t,n}^-(k) = F_{t,n}(\omega_{t,n})P_{t,n}^+(k-1)F_{t,n}^T(\omega_{t,n}) + Q_{t,n}(k),$$

Correction:

$$S_n(k) = H_n(k)P_{t,n}^-(k)H_n^T(k) + R_n(k),$$
$$K_n(k) = P_{t,n}^-(k)H_n^T(k)S_n^{-1}(k),$$
$$\boldsymbol{y}_n(k) = \boldsymbol{z}_n(k) - H_n(k)\boldsymbol{x}_{t,n}^-(k),$$
$$\boldsymbol{x}_{t,n}^+(k) = \boldsymbol{x}_{t,n}^-(k) + K_n(k)\boldsymbol{y}_n(k),$$
$$P_{t,n}^+(k) = (I - K_n(k)H_n(k))P_{t,n}^-(k),$$

in which

$$P_{t,n}^+(k) := \mathbb{E}[(\boldsymbol{x}_{t,n}(k) - \boldsymbol{x}_{t,n}^+(k))(\boldsymbol{x}_{t,n}(k) - \boldsymbol{x}_{t,n}^+(k))^T]$$

denotes the posterior estimation error covariance and $P_{t,n}^-(k)$ denotes the corresponding prior estimation error covariance, $H_n(k) = [\ldots, H_{n,i}^T(k), \ldots]^T$, $R_n(k) = diag(\ldots, R_{n,i}(k), \ldots)$, and $\boldsymbol{z}_n(k) = [\ldots, \boldsymbol{z}_{n,i}^T(k), \ldots]^T$, $\forall n \in \mathcal{N}_t$ and $i \in \mathcal{N}_s$ such that $\|\boldsymbol{p}_{t,n}(k) - \boldsymbol{p}_{s,i}(k)\| \leq r_{s,i}$. Note that $K_n(k) = O$, $\forall n \in \mathcal{N}_0(k)$, where O is a zero matrix with the corresponding dimension, and

$$\mathcal{N}_0(k) = \left\{n \in \mathcal{N}_t \middle| \|\boldsymbol{p}_{t,n}(k) - \boldsymbol{p}_{s,i}(k)\| > r_{s,i}, \forall i \in \mathcal{N}_s\right\}.$$

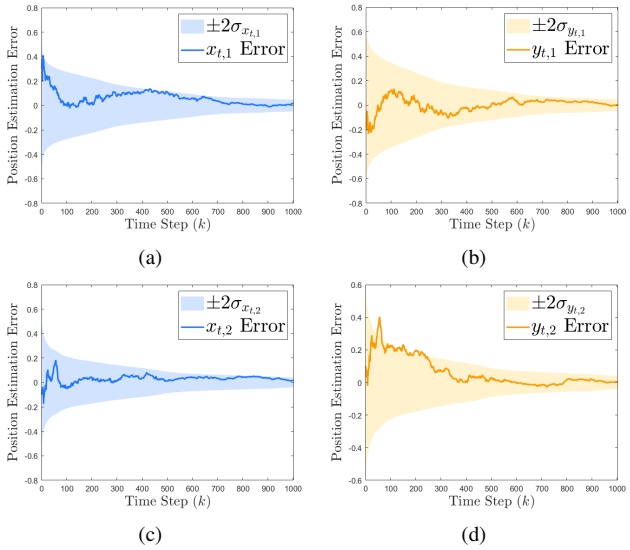

Fig. 4. Estimation errors of targets' positions and the corresponding two standard deviations along time step k. (a) Target 1's x-position estimation error; (b) Target 1's y-position estimation error; (c) Target 2's x-position estimation error; (d) Target 2's y-position estimation error.

Ideally, $f_{\boldsymbol{p}_{t,n}}^+(\boldsymbol{q}, k)$ is the probability density function of the Gaussian distribution with $\boldsymbol{x}_{t,n}(k)$ as its mean and $P_{t,n}^+(k)$ as its covariance, but the true state of a target is unknown to the robots in practice, so we approximate its mean as the posterior estimate $\boldsymbol{x}_{t,n}^+(k)$, and this approximation becomes more and more accurate as time approaches once the robots start to take measurements of the target.

B. Experimental Setup and Results

The initial conditions of the experiment are as shown in Fig. 5(a). Let $f_{pc}(r_{s,i}) = 10 \cdot r_{s,i}$, where $r_{s,1} = 0.5$, $r_{s,2} = 0.6$, $r_{s,3} = 0.7$, $r_{s,4} = 0.8$, and $r_{s,5} = 0.9$, and $\omega_{t,1} = \omega_{t,2} = -2$, $S_{\boldsymbol{\xi}_{t,1}} = S_{\boldsymbol{\xi}_{t,2}} = 3 \times 10^{-2}$. Additionally, let $H_{n,i}(k) = I \in \mathbb{R}^{4\times 4}$, $\forall n \in \mathcal{N}_t$, $i \in \mathcal{N}_s$, $\eta_{n,1} = 0.5$, $\eta_{n,2} = 0.6$, $\eta_{n,3} = 0.7$, $\eta_{n,4} = 0.8$, $\eta_{n,5} = 0.9$, $\forall n \in \mathcal{N}_t$, and $M_{n,i}(k) = diag(10, 10, 1, 1)$, $\forall n \in \mathcal{N}_t, i \in \mathcal{N}_s$. Also, we choose $N_l = 1$ to approximate (28). Strictly speaking, the theoretical validity of (39) replies on the differentiability of $\sum_{n\in\mathcal{N}_t} f_{\boldsymbol{p}_{t,n}}^+(\boldsymbol{q}, t)$ with respect to time. However, it is impossible to avoid noisy signals in practice, i.e., the differentiability of $\sum_{n\in\mathcal{N}_t} f_{\boldsymbol{p}_{t,n}}^+(\boldsymbol{q}, t)$ with respect to time does not strictly hold in practice. Nonetheless, we found in robotic implementations that one can adopt numerical methods, e.g., finite difference schemes, to approximately calculate $\frac{\partial}{\partial t}\sum_{n\in\mathcal{N}_t} f_{\boldsymbol{p}_{t,n}}^+(\boldsymbol{q}, t)$, and the smaller the sampling interval is, the better the approximation is. We set the sampling interval as 3×10^{-3}. In addition, since each robot is assumed to have a single integrator dynamics, then $m = 2$, $\boldsymbol{f}_{s,i}(\boldsymbol{p}_{s,i}) = \boldsymbol{0} \in \mathbb{R}^2$, $\boldsymbol{g}_{s,i}(\boldsymbol{p}_{s,i}) = I \in \mathbb{R}^{2\times 2}$, $\boldsymbol{f}_{s,ij}(\boldsymbol{p}_{s,ij}) = \boldsymbol{0} \in \mathbb{R}^4$, $\boldsymbol{g}_{s,ij}(\boldsymbol{p}_{s,ij}) = I \in \mathbb{R}^{4\times 4}$. Then the nominal controller $\boldsymbol{u}_s$ based on (39) needs to be perturbed in a minimally invasive manner by (15) to ensure that each robot only moves within its safe operation zone while avoiding collisions with any other robots. Let $\alpha(\hbar_{s,i}^A(\boldsymbol{p}_{s,i})) = 5 \times 10^2(\hbar_{s,i}^A(\boldsymbol{p}_{s,i}))^3$,

where $\hbar^A_{s,i}(\boldsymbol{p}_{s,i}) = \boldsymbol{p}^T_{s,i} diag(b^2_{s,i}, a^2_{s,i})\boldsymbol{p}_{s,i} - a^2_{s,i}b^2_{s,i}$, in which $a_{s,1} = a_{s,2} = 0.7$, $b_{s,1} = b_{s,2} = 0.4$, and $a_{s,3} = b_{s,3} = a_{s,4} = b_{s,4} = a_{s,5} = b_{s,5} = 0$. Additionally, let $\beta(\hbar^B_{s,ij}(\boldsymbol{p}_{s,ij})) = 1 \times 10^2(\hbar^B_{s,ij}(\boldsymbol{p}_{s,ij}))^3$, and $D_{s,ij} = 0.6$, $\forall i \neq j,\ i, j \in \mathcal{N}_s$.

The experimental results are as shown in Fig. 3, Fig. 4, and Fig. 5. The control barrier certificates defined in Section III ensure that each robot pair has a minimum safe distance such that the robots do not collide with each other, and each robot only moves within its corresponding safe operation zone, Robot 1 or Robot 2 are sometimes prevented (in a minimally perturbed manner) from approaching the centers of mass of their Voronoi cells, i.e., the critical points of the cost function $C(\boldsymbol{p}_s, t)$ defined in (17), which are inside the ellipse zone enclosed by the yellow line as shown in Fig. 5, and sometimes the robots are prevented from approaching the centers of mass of their Voronoi cells, which are located within their corresponding safe operation zones, due to the collision avoidance guarantee. These situations are expected and acceptable because the safety of multi-robot systems has priority over task accomplishments. Additionally, there exists unavoidable noise in practice. Consequently, the value of the cost function $C(\boldsymbol{p}_s, t)$ does not ideally monotonically decrease along time steps as shown in Fig. 3, but on the whole, the cost value reflects a pattern of decline.

Besides, as shown in Fig. 4, the estimation errors of the positions of Target 1 and Target 2 are both bounded and converging to zeros along time steps, which is consistent with the "shrinking" blue ellipses representing the uncertainties of the targets' positions along time steps as shown in Fig. 5, and also consistent with the tendency of the estimated trajectories approaching their corresponding true trajectories as shown in Fig. 5(l). Therefore, the effectiveness of the dynamic multi-target tracking strategy proposed in this paper is demonstrated.

VI. Conclusions

In this paper, we proposed a coverage-based simultaneous multi-target tracking and following strategy using a team of heterogeneous robots. The heterogeneous modalities are reflected by the robots' different effective sensing ranges, varied measurement noise, and diverse safe operation zones. The proposed system dynamics of the multi-robot team automatically assigns more robots to be in the area in which the targets are more likely to be, and enables the robots to dynamically and (locally) optimally cover the time-varying probability density distributions characterizing the uncertainties of the targets' positions. The single integrator dynamics model is assumed for each robot and augmented by control barrier certificates to constrain each robot to move within its safe operation zone and guarantee collision avoidance among robots. The effectiveness of the proposed dynamic multi-target tracking approach is demonstrated through an experiment performed on a team of mobile robots, where 5 heterogeneous robots are tracking and following 2 targets under noisy circular maneuvers while minimizing the uncertainties of the targets' states simultaneously.

Acknowledgment

The authors want to thank Soobum Kim for helping with the numerical algorithms for computing multiplicatively weighted Voronoi diagrams.

References

[1] C. Robin and S. Lacroix, "Multi-robot target detection and tracking: taxonomy and survey," *Autonomous Robots*, vol. 40, pp. 729–760, 2016.

[2] A. Albert and L. Imsland, "Survey: mobile sensor networks for target searching and tracking," *Cyber-Physical Systems*, vol. 4, no. 2, pp. 57–98, 2018.

[3] L. Zhou and V. Kumar, "Robust multi-robot active target tracking against sensing and communication attacks," *IEEE Transactions on Robotics*, 2023.

[4] X. R. Li and V. P. Jilkov, "Survey of maneuvering target tracking. part i. dynamic models," *IEEE Transactions on aerospace and electronic systems*, vol. 39, no. 4, pp. 1333–1364, 2003.

[5] M. Dunbabin and L. Marques, "Robots for environmental monitoring: Significant advancements and applications," *IEEE Robotics & Automation Magazine*, vol. 19, no. 1, pp. 24–39, 2012.

[6] M. Pashna, R. Yusof, Z. H. Ismail, T. Namerikawa, and S. Yazdani, "Autonomous multi-robot tracking system for oil spills on sea surface based on hybrid fuzzy distribution and potential field approach," *Ocean Engineering*, vol. 207, p. 107238, 2020.

[7] N. Bannigan, L. Orf, and E. Savory, "Tracking the centre of asymmetric vortices using wind velocity vector data fields," *Boundary-Layer Meteorology*, vol. 186, no. 1, pp. 1–26, 2023.

[8] Y. Rizk, M. Awad, and E. W. Tunstel, "Cooperative heterogeneous multi-robot systems: A survey," *ACM Computing Surveys (CSUR)*, vol. 52, no. 2, pp. 1–31, 2019.

[9] K. Zhou and S. I. Roumeliotis, "Multirobot active target tracking with combinations of relative observations," *IEEE Transactions on Robotics*, vol. 27, no. 4, pp. 678–695, 2011.

[10] S. Moon and E. W. Frew, "Distributed cooperative control for joint optimization of sensor coverage and target tracking," in *2017 International Conference on Unmanned Aircraft Systems (ICUAS)*. IEEE, 2017, pp. 759–766.

[11] M. Khaledyan, A. P. Vinod, M. Oishi, and J. A. Richards, "Optimal coverage control and stochastic multi-target tracking," in *2019 IEEE 58th Conference on Decision and Control (CDC)*. IEEE, 2019, pp. 2467–2472.

[12] S. Thrun, "Probabilistic robotics," *Communications of the ACM*, vol. 45, no. 3, pp. 52–57, 2002.

[13] A. D. Ames, S. Coogan, M. Egerstedt, G. Notomista, K. Sreenath, and P. Tabuada, "Control barrier functions: Theory and applications," in *2019 18th European control conference (ECC)*. IEEE, 2019, pp. 3420–3431.

[14] S. Kim and M. Egerstedt, "Heterogeneous coverage control with mobility-based operating regions," in *2022 American Control Conference (ACC)*. IEEE, 2022, pp. 2148–2153.

[15] H. Mahboubi and A. G. Aghdam, "Distributed deployment algorithms for coverage improvement in a network of wireless mobile sensors: Relocation by virtual force," *IEEE Transactions on Control of Network Systems*, vol. 4, no. 4, pp. 736–748, 2016.

[16] S. Kim, M. Santos, L. Guerrero-Bonilla, A. Yezzi, and M. Egerstedt, "Coverage control of mobile robots with different maximum speeds for time-sensitive applications," *IEEE Robotics and Automation Letters*, vol. 7, no. 2, pp. 3001–3007, 2022.

[17] R. Lin and M. Egerstedt, "Coverage control on the special euclidean groups," in *2023 American Control Conference (ACC)*. IEEE, 2023, pp. 1972–1979.

[18] H. Flanders, "Differentiation under the integral sign," *The American Mathematical Monthly*, vol. 80, no. 6, pp. 615–627, 1973.

[19] S. G. Lee, Y. Diaz-Mercado, and M. Egerstedt, "Multirobot control using time-varying density functions," *IEEE Transactions on robotics*, vol. 31, no. 2, pp. 489–493, 2015.

[20] B. Boots, K. Sugihara, S. N. Chiu, and A. Okabe, "Spatial tessellations: concepts and applications of voronoi diagrams," 2009.

[21] S. Wilson, P. Glotfelter, L. Wang, S. Mayya, G. Notomista, M. Mote, and M. Egerstedt, "The robotarium: Globally impactful opportunities, challenges, and lessons learned in remote-access, distributed control of multirobot systems," *IEEE Control Systems Magazine*, vol. 40, no. 1, pp. 26–44, 2020.

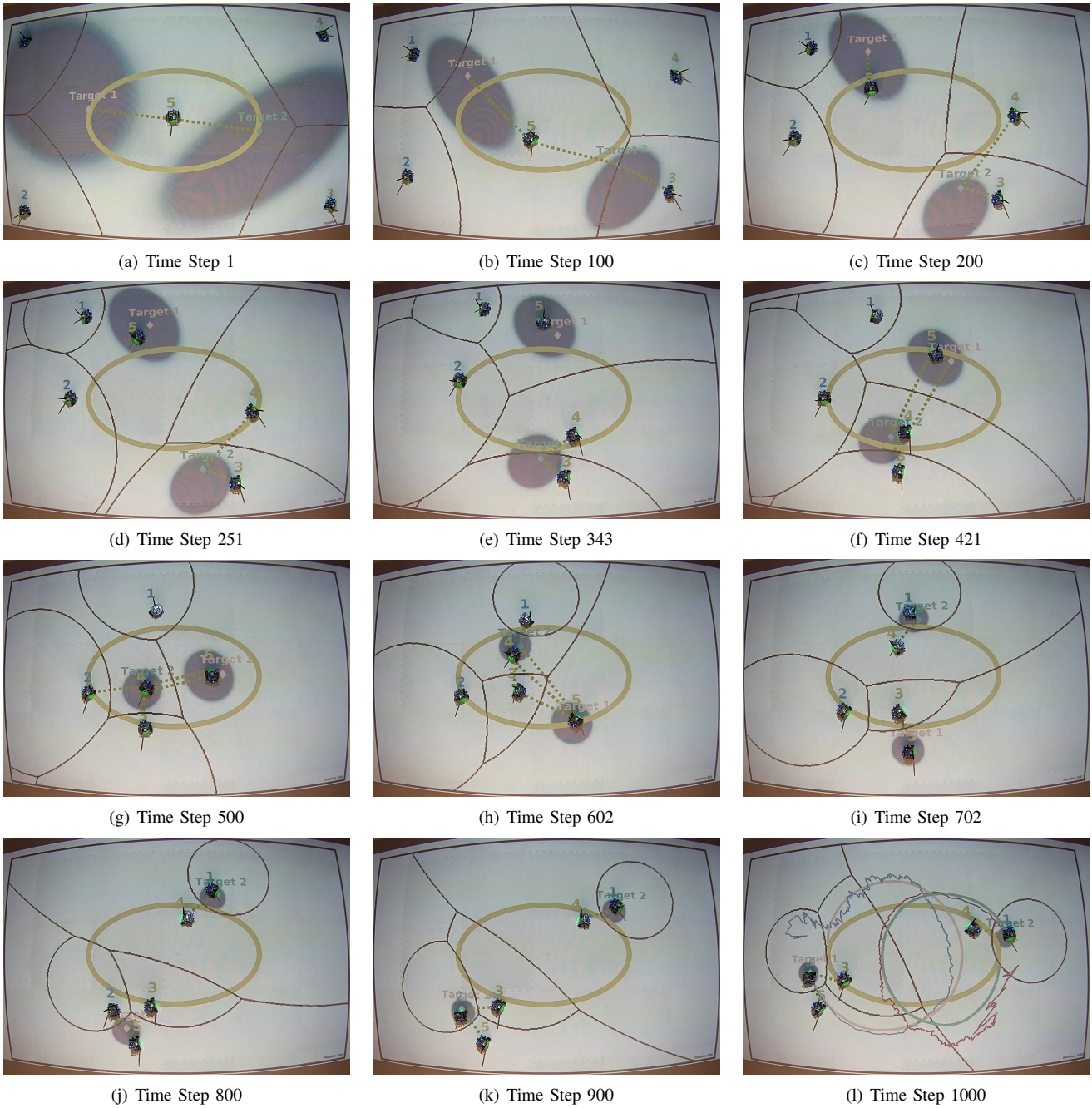

(a) Time Step 1 (b) Time Step 100 (c) Time Step 200

(d) Time Step 251 (e) Time Step 343 (f) Time Step 421

(g) Time Step 500 (h) Time Step 602 (i) Time Step 702

(j) Time Step 800 (k) Time Step 900 (l) Time Step 1000

Fig. 5. The process of a team of 5 robots, with the blue-labeled Robots 1 and 2 having similar operation zones to the two ground robots illustrated in Fig. 1 and the yellow-labeled Robots 3, 4 and 5 having similar operation zones to the three quadrotors illustrated in Fig. 1, tracking Target 1 and Target 2, whose true positions are represented by the pink and aquamarine diamonds respectively. The green dashed line connecting a target and a robot represents that the target is within the robot's effective sensing region and taken measurements by the robot. The probability density distributions characterizing the uncertainties of the targets' positions are represented by the blue ellipses. Each robot has a dominant region, i.e., a multiplicatively weighted Voronoi cell, with a set of black curves as its boundary. The ellipse zone located at the center and enclosed by the yellow line is similar to the hill as shown in Fig. 1, and is the unsafe operation zone for Robots 1 and 2. In the figure of time step 1000, the pink, aquamarine, blue, and magenta trajectories represent the true trajectory of Target 1, the true trajectory of Target 2, the estimated trajectory of Target 1, and the estimated trajectory of Target 2, respectively.